

Bayesian inference for stochastic oscillatory systems using the phase-corrected Linear Noise Approximation

Ben Swallow^{*}, David A. Rand and Giorgos Minas[‡]

Abstract. Likelihood-based inference in stochastic non-linear dynamical systems, such as those found in chemical reaction networks and biological clock systems, is inherently complex and has largely been limited to small and unrealistically simple systems. Recent advances in analytically tractable approximations to the underlying conditional probability distributions enable long-term dynamics to be accurately modelled, and make the large number of model evaluations required for exact Bayesian inference much more feasible. We propose a new methodology for inference in stochastic non-linear dynamical systems exhibiting oscillatory behaviour and show the parameters in these models can be realistically estimated from simulated data. Preliminary analyses based on the Fisher Information Matrix of the model can guide the implementation of Bayesian inference. We show that this parameter sensitivity analysis can predict which parameters are practically identifiable. Several Markov chain Monte Carlo algorithms are compared, with our results suggesting a parallel tempering algorithm consistently gives the best approach for these systems, which are shown to frequently exhibit multi-modal posterior distributions.

MSC2020 subject classifications: Primary 62-08, 62F15, 60K35; secondary 62P10.

Keywords: sensitivity analysis, parameter identifiability, SDEs, linear noise approximation, oscillations.

1 Introduction

Oscillations are abundant in biology, ecology, epidemiology, and other applied fields (Goldental et al., 2017). Exdosomeles include genetic oscillations observed in biological systems (Forger, 2017; Gonze and Ruoff, 2021) such as the circadian clock (Gonze et al., 2003), embryonic development (Marinopoulou et al., 2021), cell signalling (Ashall et al., 2009), predator-prey oscillations in ecology (Gard and Kannan, 1976; Froda and Nkurunziza, 2007), and epidemic oscillations (Greer et al., 2020; Weitz et al., 2020). Dynamical systems presenting oscillations naturally carry more information than stable systems through their period, phase, and doselitude components. To capture this information, one needs to observe their dynamics over time, rather than through a single

arXiv: 2010.00000

^{*}School of Mathematics and Statistics, University of Glasgow, Glasgow, UK ben.swallow@glasgow.ac.uk

[†]Mathematics Institute, University of Warwick, Coventry, UK d.a.rand@warwick.ac.uk

[‡]School of Mathematics and Statistics, University of St Andrews, St Andrews, UK gm256@st-andrews.ac.uk

static observation. Time-series data are therefore important for prediction and for inference on the parameters of oscillatory models. Cutting-edge technology in molecular biology, such as fluorescent imaging and sequencing [Gabriel et al. \(2021\)](#); [Lane et al. \(2017\)](#); [DeFelice et al. \(2019\)](#), and ecology (e.g. wearable devices, GPS, cameras), and widespread surveillance of seasonal epidemics, and elsewhere, provide such time-series observations.

Traditionally oscillations are modelled by deterministic dynamical systems, often described by ordinary differential equations. However, a key component of oscillatory systems is that they are often stochastic by nature ([Boettiger, 2018](#); [Ashall et al., 2009](#); [Gonze et al., 2003](#); [Allen, 2017](#)). For instance, systems in molecular biology evolve through biochemical reactions affected by the stochastic movement of molecules in biological cells ([Gillespie, 1977](#); [VAN KAMPEN, 2007](#); [Wilkinson, 2011](#); [Lei, 2021](#)). This intrinsic stochasticity is reflected in time-series data that are typically highly variable across individuals or at different times ([Ashall et al., 2009](#); [Gabriel et al., 2021](#)). Deterministic models fail to capture this intrinsic stochasticity of oscillatory systems providing poor fit to data and poor parameter estimation ([Ashall et al., 2009](#); [Harper et al., 2018](#); [Tay et al., 2010a](#)).

Stochastic models are therefore necessary for parameter estimation using highly-variable time-series data. These are continuous-time Markov processes, which are typically non-homogeneous as the transition propensities depend on the current state of the system. A range of approaches for stochastic modelling are available. The model that is considered to be exact (under generic assumptions) in the context of biochemical reactions is the so-called Chemical Master Equation (CME) ([Gillespie, 1992](#); [Wilkinson, 2011](#); [Lei, 2021](#)). The well-known Stochastic Simulation Algorithm (SSA), also called the Gillespie algorithm, allows for exact simulation from the CME model and it is widely used for stochastic simulation in many fields ([Gillespie, 1992](#)). However, the likelihood of the CME model is analytically intractable in most situations. Therefore the use of simulation-based methods, such as Approximate Bayesian Computation (ABC), is required to perform parameter inference ([Beaumont, 2003](#); [Sisson et al., 2018](#); [Wilkinson, 2011](#)).

Less progress has been made in parameter estimation when the dynamics of the system are non-linear (for instance oscillatory), despite there being a wide variety of approximate models enabling faster simulation ([Gillespie and Petzold, 2003](#); [Gillespie, 2000](#)). One such method, the Linear Noise Approximation (LNA) of the CME ([VAN KAMPEN \(2007\)](#); [Kurtz \(1970\)](#)), described by Stochastic Differential Equations (SDEs), provides analytically tractable likelihood computation of time-series observations ([Komorowski et al. \(2009\)](#); [Fearnhead et al. \(2014\)](#); [Minas and Rand \(2017\)](#); [Schnoerr et al. \(2017\)](#); [Finkenstädt et al. \(2013\)](#); [Girolami and Calderhead \(2011\)](#)), but fails to accurately model oscillators ([Minas and Rand \(2017\)](#); [Ito and Uchida \(2010\)](#)). An extension of the LNA, called phase corrected LNA or pcLNA ([Minas and Rand, 2017](#)), can accurately simulate oscillatory dynamics of the CME. This method takes advantage of the stability of oscillatory systems in directions transversal to the oscillations, and corrects for the uncontrolled variation of the phase of oscillators. The pcLNA framework provides simulation algorithms that remain accurate for long simulated trajectories and are fast

in implementation thus making exact parameter estimation methods such as Markov chain Monte Carlo (MCMC) feasible. The method also allows for computing information theoretic quantities such as the Fisher Information to study the model’s parameter sensitivities, quantities that can be vital for efficient and reliable parameter estimation in such complex systems.

An important characteristic of oscillatory systems is that they typically involve a large number of variables and parameters. For instance, the model of the circadian clock of *Drosophila.Melanogaster* and the NF- κ B signalling system that we consider here involve 10 and 11 variables, and 39 and 30 parameters, respectively. These systems describe the biochemical evolution of the certain molecular populations over time. The transitions include reactions (e.g. transcription, translation, degradation, and phosphorylation) and translocations, and the parameters to be estimated include constants describing the speed of reactions, and threshold values for non-linear reactions. It is well-known that deterministic models for these systems face substantial parameter identifiability issues (“sloppiness”) in practice (Gutenkunst et al., 2007; Rand, 2008; Minas and Rand, 2019a; Browning et al., 2020), with further challenges being proposed by stochastic models.

This paper considers the use of Bayesian parameter estimation methods to estimate the parameters of a stochastic dynamical system approximated using the pcLNA method based on time series observations. Our approach has three main purposes. Firstly, to perform parameter sensitivity analysis for systems with a large number of parameters to identify the parameters that the system is more sensitive to. Secondly, to describe a Kalman Filter that can be used to derive the likelihood of time-series observations under the proposed model. Third, to apply and compare different Bayesian computational methods, in particular MCMC methods, in order to examine their performance. We will use the information derived from the parameter sensitivity analysis to target selected parameters, and examine whether this targeted approach is more successful than non-targeted approaches. We develop and apply MCMC computational methods, more specifically random-walk Metropolis Hastings (RWMH), a simplified manifold Metropolis-adjusted Langevin algorithm (SMMALA) and a parallel tempered MCMC, to derive posterior distributions of parameters using time series data.

We find that the results of the parameter identifiability study are reflected into the Markov chains’ properties, in the sense that parameters that are suggested as non-identifiable in our study are seen to have issues of non-convergence, and poor mixing, or at best minimal posterior concentration relative to the prior. This, to a large extent, is regardless of the computational method used. On the contrary, the parameters that are identifiable according to our study, appear to converge and mix well in the MCMC methods. We also perform a comparison between the MCMC methods and provide a variety of experimental conditions to test the approach, such as different systems and stochasticity levels in the data. Overall, the parallel tempering method is found to perform best, in terms of convergence, particularly dealing with multi-modal distributions.

Previous studies (Komorowski et al., 2009; Finkenstädt et al., 2013; Girolami and Calderhead, 2011) have examined the use of Bayesian methods to estimate parameters of the LNA model. Here we consider the use of those methods for oscillatory dynamics

where the LNA model is inaccurate. [Fearnhead et al. \(2014\)](#) uses a similar approach in improving the accuracy of the LNA, by applying frequent corrections to the initial conditions of the ODEs used to solve the LNA system equations forward in time. As we explain in section 3, the pcLNA method takes advantage of the oscillatory dynamics by correcting only the time/phase of a pre-computed solution of the LNA equations, which leads to a significant decrease in the implementation time. The pcLNA approach also allows for the computation of the Fisher Information without significant increase in computational time compared to the standard LNA model. Therefore, a parameter sensitivity analysis based on Fisher Information can be performed and in turn guide parameter estimation of oscillatory systems.

1.1 Exemplar systems

In order to test the methodology, we apply the methods developed in this paper to two biological systems. Both of these systems present oscillations generated by negative feedback loops with large numbers of parameters and variables.

Our first exemplar system is that of the NF- κ B signalling system in mammalian cells. The NF- κ B system regulates cell response to stress and inflammation, and its dysregulation plays a key role in autoinflammatory diseases, cancer, and other pathological conditions ([Zhang et al., 2017](#)). We utilise an 11-dimensional system corresponding to a reduced version of the model of [Ashall et al. \(2009\)](#) as described in [Minas and Rand \(2017\)](#). It describes the oscillatory response of the NF- κ B system following stimulation by the cytokine tumor necrosis factor alpha (TNF α). Continuous stimulation of the system causes a transient oscillation that quickly relaxes to a stable limit cycle. The NF- κ B system has been shown to be highly stochastic [Tay et al. \(2010b\)](#). The model in [Ashall et al. \(2009\)](#) involves reactions modelled by both linear and non-linear functions, with a total of 31 parameters including reaction rate constants, and Michaelis-Menten or Hill equation constants. Estimation of those parameters is extremely important for developing greater understanding of the biology of the system.

For the same reason we also consider the circadian clock model developed in [Gonze et al. \(2003\)](#) for *Drosophila.Melanogaster*. The system involves 30 reactions parameterised by 38 parameters of similar types as the NF- κ B model. The system is shown to present sustained oscillations generated by negative feedback loops (self-inhibition of gene expression). [Minas and Rand \(2019b\)](#) analysed this system and showed a substantially higher parameter sensitivity of the stochastic model described below, compared to the deterministic model of this system. Higher relative sensitivity is presented in this system compared to the NF- κ B system as described below.

2 System sensitivity analysis and identifiability

Due to the coupling between the variables of non-linear dynamical systems in biology, it is frequently the case that parameters are fully or partially non-identifiable. Local sensitivity metrics such as Fisher information enable a study of parameter identifiability

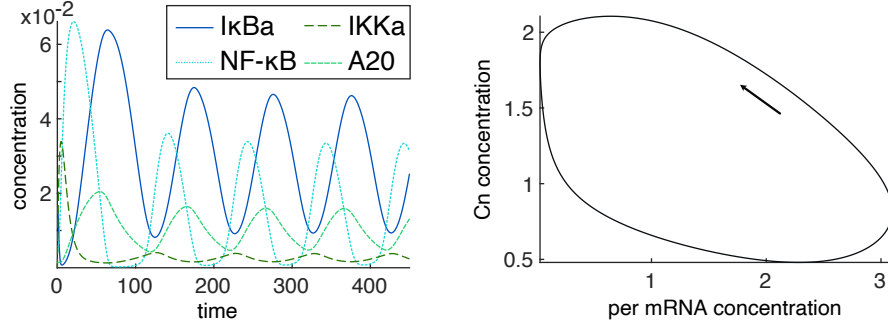


Figure 1: The dynamics of the exemplar systems. a. The (deterministic) solutions of the NF- κ B system responding to a continuous TNF α stimulation plotted against time. Here only 4 variables are presented, specifically the concentrations of the inhibitor protein I κ B α in the cytoplasm, the NF- κ B concentration in the nucleus, the concentration of the active kinase of the inhibitor IKKa, and of the A20 protein. Observe that the I κ B α is negatively correlated with NF- κ B, same with A20 and IKKa. b. The solutions of the Drosophila circadian clock. Two variables are presented and plotted against each other. These are the mRNA expression levels of per gene, and the concentration of its inhibitor, C_n , which is a complex formed by a (phosphorylated) form of proteins Per and Tim. The direction of time-evolution of the system is indicated by an arrow.

in the system and can therefore provide an *a priori* indication of which parameter(s) are identifiable.

Fisher Information

Fisher Information quantifies the information that an observable random variable carries about an unknown parameter θ . If $P(\mathbf{X}; \theta)$ is the probability density function of a continuous random vector \mathbf{X} depending on parameter vector θ , the Fisher Information Matrix (FIM) $I = I_P$ has entries

$$I_{ij} = E \left[\frac{\partial \ell}{\partial \theta_i} \frac{\partial \ell}{\partial \theta_j} \right] = -E \left[\frac{\partial^2 \ell(\theta; \mathbf{X})}{\partial \theta_i \partial \theta_j} \right], \quad (2.1)$$

where $\ell = \log P$, and θ_i and θ_j are the i th and j th components of the parameter vector θ . If P is Multivariate Normal (MVN) with mean $\boldsymbol{\mu} = \boldsymbol{\mu}(\theta)$ and covariance $\boldsymbol{\Sigma} = \boldsymbol{\Sigma}(\theta)$ then

$$I_{ij} = \frac{\partial \boldsymbol{\mu}^T}{\partial \theta_i} \boldsymbol{\Sigma}^{-1} \frac{\partial \boldsymbol{\mu}}{\partial \theta_j} + \frac{1}{2} \text{tr} \left(\boldsymbol{\Sigma}^{-1} \frac{\partial \boldsymbol{\Sigma}}{\partial \theta_i} \boldsymbol{\Sigma}^{-1} \frac{\partial \boldsymbol{\Sigma}}{\partial \theta_j} \right). \quad (2.2)$$

The FIM measures the sensitivity of P to a change in parameters in the sense that

$$D_{KL}(P(\cdot, \theta + \delta\theta), P(\cdot, \theta)) = \frac{1}{2} \delta\theta^T I_P \delta\theta + O(\|\delta\theta\|^3)$$

where D_{KL} is the Kullback-Leibler divergence. The significance of the FIM for sensitivity and experimental design follows from its role in (2.1) as an approximation to the Hessian of the log-likelihood function at a maximum. Assuming non-degeneracy, if θ^* is a parameter value of maximum likelihood there is a $s \times s$ orthogonal matrix \mathbf{A} such that, in the new parameters $\theta' = \mathbf{A} \cdot (\theta - \theta^*)$,

$$\ell(\theta) \approx \ell(\theta^*) - \sum_i \sigma_i^2 \theta_i'^2.$$

for θ near θ^* . From these facts it follows that the σ_i^2 are the eigenvalues of the FIM and that the matrix V diagonalises it. If we assume that the σ_i are ordered so that $\sigma_1^2 \geq \dots \geq \sigma_s^2$ then it follows that near the maximum the likelihood is most sensitive when θ'_1 is varied and least sensitive when θ'_s is. Moreover, σ_i is a measure of this sensitivity.

Because the FIM $\mathcal{I} = \mathcal{I}(\theta)$ is symmetric and positive semi-definite, its Singular Value Decomposition (SVD) is of the form VD^2V^T where V is orthogonal and D is diagonal with entries $\sigma_1 \geq \dots \geq \sigma_s \geq 0$. It can therefore be decomposed to $\mathcal{I} = \underline{\mathbf{s}}^T \underline{\mathbf{s}}$ with the matrix $\underline{\mathbf{s}} = \underline{\mathbf{s}}(\theta) = DV^T$ and the KL divergence

$$D_{KL}(P_{\theta+\delta\theta}||P_\theta) = \frac{1}{2} \|\underline{\mathbf{s}} \delta\theta\|^2 + O(\|\delta\theta\|^3) = \frac{1}{2} \sum_{i,j,l} \delta\theta_j \delta\theta_l \underline{\mathbf{s}}_{ij} \underline{\mathbf{s}}_{il} + O(\|\delta\theta\|^3). \quad (2.3)$$

The length, $\|\underline{\mathbf{s}}_j\|^2$, of the column $\underline{\mathbf{s}}_j = (\underline{\mathbf{s}}_{1j}, \dots, \underline{\mathbf{s}}_{kj})^T$ of $\underline{\mathbf{s}}$, measures the effects of a single unit change of the j -th parameter θ_j to the distribution P_θ , $j = 1, \dots, k$. It can therefore be used to study the sensitivity of P_θ to changes in the parameter values.

3 The pLNA model

We first describe the standard Linear Noise Approximation (LNA) model and then proceed with the phase corrected LNA model. The LNA model considers the evolution of a system of N interacting populations over time. The state of the system, $\mathbf{X}(t) = (X_1(t), \dots, X_N(t))^T$, at time $t > 0$ is given by

$$\mathbf{X}(t) = \boldsymbol{\varphi}(t) + \Omega^{-1/2} \boldsymbol{\xi}(t). \quad (3.1)$$

Here $\boldsymbol{\varphi}(t) = \boldsymbol{\varphi}(t; \theta)$ is a (deterministic) solution of the ODE

$$d\boldsymbol{\varphi} = \mathbf{F}(\boldsymbol{\varphi})dt = \mathbf{A}\mathbf{r}(\boldsymbol{\varphi})dt, \quad (3.2)$$

and $\boldsymbol{\xi}_t = \boldsymbol{\xi}(t)$ the solution of the SDE

$$d\boldsymbol{\xi}_t = \mathbf{J}\boldsymbol{\xi}_t dt + \mathbf{S}d\mathbf{W}_t. \quad (3.3)$$

Here we define the following terms.

- $\mathbf{A} = [\mathbf{a}_1 \dots \mathbf{a}_R]$ is the $N \times R$ stoichiometry (or transition) matrix of the system and $\mathbf{r}(\boldsymbol{\varphi}) = (r_1(\boldsymbol{\varphi}), \dots, r_R(\boldsymbol{\varphi}))'$, with the column \mathbf{a}_j representing the state change after the occurrence of the j -th transition that occurs with rate $r_j(\boldsymbol{\varphi})$, $j = 1, \dots, R$.

- The drift matrix of the SDE in (3.3) is the Jacobian matrix of the system in (3.2), i.e. $\mathbf{J} = \mathbf{J}(\boldsymbol{\varphi}(t)) = (dF_i(\boldsymbol{\varphi}(t))/d\varphi_j)_{i,j}$, while $\mathbf{S}^2 = \mathbf{S}(\boldsymbol{\varphi}(t))^2 = \mathbf{A}\mathbf{R}(\boldsymbol{\varphi}(t))\mathbf{A}'$ with $\mathbf{R}(\boldsymbol{\varphi})$ a diagonal matrix with main diagonal $\mathbf{r}(\boldsymbol{\varphi})$. The stochastic process $\{\mathbf{W}_t : t \geq 0\}$ is a classical Wiener process.
- The scaling parameter Ω , often called system size, is typically considered as a known fixed value of the system (e.g. cell volume, total population size). It is not necessary to identify such a parameter (i.e. it can be fixed to 1), but in some cases, in particular for the NF- κ B system that we consider, the parameter has been estimated for certain cell types.

The SDE in (3.3) can be solved analytically, with the solution satisfying

$$\boldsymbol{\xi}_t = \mathbf{C}(t_0, t)\boldsymbol{\xi}_{t_0} + \boldsymbol{\eta}_t, \quad \boldsymbol{\eta}_t \sim N(0, \mathbf{V}(t_0, t)). \quad (3.4)$$

Here the matrices \mathbf{C} and \mathbf{V} are solutions of the initial value problems,

$$\dot{\mathbf{C}} = d\mathbf{C}/dt = \mathbf{J}\mathbf{C}, \quad \mathbf{C}(t_0, t_0) = \mathbf{I}, \quad (3.5)$$

$$\dot{\mathbf{V}} = d\mathbf{V}/dt = \mathbf{J}\mathbf{V} + \mathbf{V}\mathbf{J}^T + \mathbf{S}, \quad \mathbf{V}(t_0, t_0) = \mathbf{0} \quad (3.6)$$

where the matrices $\mathbf{J} = \mathbf{J}(\boldsymbol{\varphi}(t))$ and $\mathbf{S} = \mathbf{S}(\boldsymbol{\varphi}(t))$ are defined above.

Equation (3.4) implies that, if the initial condition $\boldsymbol{\xi}_{t_0}$ has MVN distribution, the transition probabilities of the LNA model, say $P(\mathbf{X}(t_1)|\mathbf{X}(t_0))$, for $t_1 > t_0$ are MVN. We can also show that the joint probability distribution of time series observations $(\mathbf{X}(t_0), \mathbf{X}(t_1), \dots, \mathbf{X}(t_n))$ are multivariate normal with precision matrix that has a tridiagonal form. Practically, using the LNA involves solving the ODE system in (3.2) for appropriate initial conditions, and then using this solution $\boldsymbol{\varphi}(t)$ to compute the matrices $\mathbf{J} = \mathbf{J}(\boldsymbol{\varphi}(t))$ and $\mathbf{S} = \mathbf{S}(\boldsymbol{\varphi}(t))$, and solve (3.5), and (3.6). The solutions $\boldsymbol{\varphi}(t)$, $\mathbf{C}(t, t_0)$, $\mathbf{V}(t, t_0)$, $t \in [t_0, T]$ can be used for deriving the probability distribution of the state of the system, performing simulations, computing the FIM of the model parameters, statistical inference (see below), and other purposes.

The accuracy of the standard LNA model, when compared to the Chemical Master Equation (CME) model either analytically or through Gillespie simulations, is found to depend on the system dynamics, and the relation between Ω and $T - t_0$, i.e. the length of the time-interval to be described. For instance, the LNA model is shown to be accurate for long-times when describing the dynamics of a stochastic dynamical system that has reached the neighborhood of an equilibrium of the system in (3.2). An accurate LNA can also be derived for any system when for a given Ω , the length of the time-interval is chosen to be sufficiently short (see Grima et al. (2011), Wallace et al. (2012)). However, it is inaccurate in describing the long-time behaviour of stochastic systems presenting oscillations. For instance, we found that the standard LNA model is inaccurate when describing the NF- κ B and circadian clock oscillations even for time-intervals less than one oscillation cycle (Minas and Rand (2017)).

By studying the dynamics of oscillatory systems that present attractive limit cycles, the phase corrected LNA model (pcLNA) takes advantage of the stability of these

systems in all-but-one directions of the state space. That is, these systems are stable in the $N - 1$ transversal directions to the limit cycle. The variation in the unstable tangential direction can be controlled by frequently correcting the phase of the system. The frequency depends on the dynamics of the system and the scale of stochasticity (here expressed by parameter Ω). Minas and Rand (2017) observed that about 3-4 corrections per oscillation cycle was sufficient for the NF- κ B system and the *Drosophila* circadian clock model ($\Omega \in (300, 2000)$).

For a system with limit cycle solution, $\varphi(t)$, $t \in [0, \pi]$, with period π , the pcLNA model is

$$\mathbf{X}(t) = \varphi(s_0 + (t - t_0)) + \Omega^{-1/2} \boldsymbol{\xi}(s_0 + (t - t_0)) \quad (3.7)$$

where

- $s_0 \in [0, \pi]$ is selected so that $\varphi(s_0)$ is the closest point to the current state $\mathbf{X}(t_0)$, i.e.

$$\varphi(s_0) = \Phi(\mathbf{X}(t_0)) := \arg \min_{\varphi(s), s \in [0, \pi]} D(\mathbf{X}(t_0), \varphi(s)), \quad (3.8)$$

for some distance metric D .

- $\boldsymbol{\xi}(t)$ is the solution of the SDE in (3.3) with initial condition

$$\boldsymbol{\xi}(s_0) = \boldsymbol{\kappa}_0 := \Omega^{1/2}(\mathbf{X}(t_0) - \varphi(s_0)). \quad (3.9)$$

If the distance function D is Euclidean, the point $\mathbf{X}(t_0)$ lies on the orthogonal transversal section of the limit cycle $\varphi(t)$ at $\varphi(s_0)$. The point $\varphi(s_0)$ can then be easily found for instance by an optimization method, such as the Newton-Raphson method. Note that only a single solution for the LNA system equations, i.e. the ODE systems in eqs. (3.2), (3.5) and (3.6), is used in defining the pcLNA model in eqs. (3.7) to (3.9).

3.1 The pcLNA Kalman Filter

The Kalman Filter is used to derive the likelihood of time-series $\mathbf{y} = (\mathbf{y}_0, \mathbf{y}_1, \dots, \mathbf{y}_N)$ where $\mathbf{y}_i = \mathbf{y}(t_i)$ is the observation at time t_i , $i = 0, 1, \dots, N$. The likelihood can be factorised as

$$L(\boldsymbol{\theta}; \mathbf{y}) = P(\mathbf{y}_0; \boldsymbol{\theta}) \prod_{i=1}^N P(\mathbf{y}_i | \mathbf{y}_{i-1}; \boldsymbol{\theta}).$$

The Kalman Filter is a recursive algorithm that uses the model's transition equations and Bayes rule to repeatedly perform the transition from prior to posterior distributions (i.e. $(\cdot | \mathbf{y}_{i-1})$ and $(\cdot | \mathbf{y}_i)$) to obtain the likelihood factors $P(\mathbf{y}_{i+1} | \mathbf{y}_i; \boldsymbol{\theta})$, for $i = 1, 2, \dots, N - 1$.

The pcLNA Kalman Filter transitions are governed by the following equations. For $i = 1, \dots, N$,

$$\text{(Observation)} \quad \mathbf{Y}_i = \mathbf{Y}(t_i) = \mathbf{B}\mathbf{X}_i + \boldsymbol{\epsilon}_i, \quad \boldsymbol{\epsilon}_i \sim N(0, \boldsymbol{\Sigma}_e), \quad \boldsymbol{\epsilon}_i \perp \mathbf{X} \quad (3.10)$$

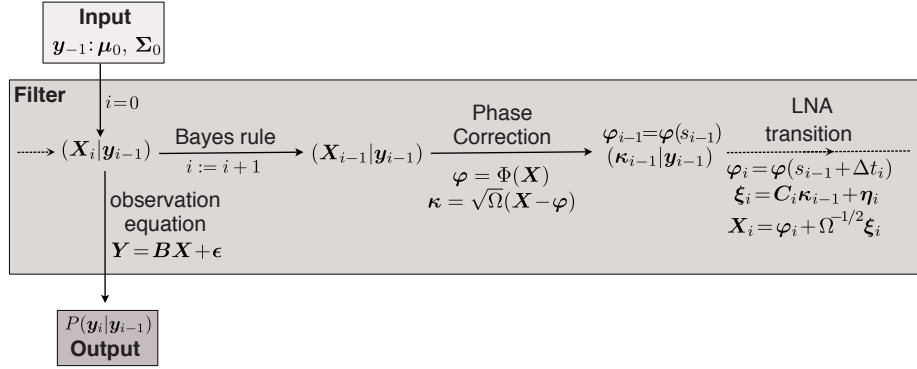


Figure 2: Kalman filter for the pcLNA algorithm.

$$\text{(State)} \quad \mathbf{X}_i = \mathbf{X}(t_i) = \boldsymbol{\varphi}_i + \Omega^{-1/2} \boldsymbol{\xi}_i, \quad (3.11)$$

$$\text{(Phase correction)} \quad \boldsymbol{\varphi}_i = \boldsymbol{\varphi}(s_i) := \boldsymbol{\Phi}(\mathbf{X}_i), \quad \boldsymbol{\kappa}_i = \Omega^{1/2}(\mathbf{X}_i - \boldsymbol{\varphi}_i) \quad (3.12)$$

$$\text{(Transition)} \quad \boldsymbol{\varphi}_{i+1} = \boldsymbol{\varphi}(s_{i+1}), \quad s_{i+1} = s_i + \Delta t_i, \quad \Delta t_{i+1} = t_{i+1} - t_i \quad (3.13)$$

$$\boldsymbol{\xi}_{i+1} = \mathbf{C}(s_i, s_{i+1}) \boldsymbol{\kappa}_i + \boldsymbol{\eta}_{i+1}, \quad \boldsymbol{\eta}_{i+1} \sim N(0, \mathbf{V}(s_i, s_{i+1})), \quad (3.14)$$

The matrix \mathbf{B} in the observation equation (3.10) is a constant $q \times n$ matrix that determines how the observation relates to the underlying stochastic process. For exdosele, \mathbf{B} might eliminate unobserved variables in \mathbf{X} . Note also that the pcLNA Kalman Filter uses the pre-computed solutions of the initial value problems in eqs. (3.2), (3.5) and (3.6) of the LNA, which we respectively denote $\boldsymbol{\varphi}(t)$, $\mathbf{C}(t_0, t)$, $\mathbf{V}(t_0, t)$, $t_0 \leq t < T$.

We now outline the steps of the pcLNA Kalman Filter algorithm. We use the notation $P_N(\cdot | \mathbf{m}, \mathbf{S})$ to denote the pdf of a MVN distribution with mean vector \mathbf{m} and variance matrix \mathbf{S} . The mean and variance of observation \mathbf{y}_i are denoted by $\{\boldsymbol{\mu}_i^{(\mathbf{Y})}, \boldsymbol{\Sigma}_i^{(\mathbf{Y})}\}$, prior means and variances of $(\mathbf{X}_i | \mathbf{y}_{i-1})$ and $(\boldsymbol{\kappa}_i | \mathbf{y}_{i-1})$ by $\{\boldsymbol{\mu}_i, \boldsymbol{\Sigma}_i\}$ and $\{\mathbf{m}_i, \mathbf{S}_i\}$, with the symbol * denoting the corresponding posterior parameters.

(KF1) **Input** $(\mathbf{y}_0, \mathbf{y}_1, \dots, \mathbf{y}_N)$, $\boldsymbol{\mu}_0$, $\boldsymbol{\Sigma}_0$, \mathbf{B} and $\boldsymbol{\Sigma}_e$.

(KF2) Compute $\boldsymbol{\mu}_0^{(\mathbf{Y})} = \mathbf{B}\boldsymbol{\mu}_0$, $\boldsymbol{\Sigma}_0^{(\mathbf{Y})} = \boldsymbol{\Sigma}_0 + \boldsymbol{\Sigma}_e$. **Output:** $P(\mathbf{y}_0; \boldsymbol{\theta}) = P_N(\mathbf{y}_0 | \boldsymbol{\mu}_0^{(\mathbf{Y})}, \boldsymbol{\Sigma}_0^{(\mathbf{Y})})$.

(KF3) For iteration $i = 1, 2, \dots, N - 1$

(KF3a) Compute the posterior mean and variance of $(\mathbf{X}_{i-1} | \mathbf{y}_{i-1})$

$$\boldsymbol{\mu}_{i-1}^* = \boldsymbol{\mu}_{i-1} + \boldsymbol{\Sigma}_{i-1} \mathbf{B}^T (\boldsymbol{\Sigma}_{i-1}^{(\mathbf{Y})})^{-1} \hat{\boldsymbol{\epsilon}}_{i-1}, \quad \hat{\boldsymbol{\epsilon}}_{i-1} = \mathbf{y}_{i-1} - \boldsymbol{\mu}_{i-1}^{(\mathbf{Y})}$$

$$\Sigma_{i-1}^* = \Sigma_{i-1} - \Sigma_{i-1} \mathbf{B}^T (\Sigma_{i-1}^Y)^{-1} \mathbf{B} \Sigma_{i-1}$$

(KF3b) Compute $\varphi_{i-1} := \varphi(s_{i-1}) = \Phi(\boldsymbol{\mu}_{i-1}^*)$ and the posterior mean and variance of $(\boldsymbol{\kappa}_{i-1} | \mathbf{y}_{i-1})$

$$\begin{aligned} \mathbf{m}_{i-1}^* &= \Omega^{1/2} (\boldsymbol{\mu}_{i-1}^* - \varphi_{i-1}) \\ \mathbf{S}_{i-1}^* &= \Omega \mathbf{E}_2 \left(\Sigma_{22,i-1}^* - \frac{(\Sigma_{12,i-1}^*)^T \Sigma_{12,i-1}^*}{\Sigma_{11,i-1}^*} \right) \mathbf{E}_2^T \end{aligned}$$

where $\mathbf{E}_2 := [e_2 \cdots e_n]$ with $e_j^T e_{j'} = 0$, $j, j' \in \{1, 2, \dots, n\}$, and $\mathbf{e}_1 := \mathbf{F}(\varphi_{i-1})$. Here

$$\Sigma_{11,i-1}^* = e_1^T \Sigma_{i-1}^* e_1, \quad \Sigma_{12,i-1}^* = e_1^T \Sigma_{i-1}^* \mathbf{E}_2, \quad \Sigma_{22,i-1}^* = \mathbf{E}_2^T \Sigma_{i-1}^* \mathbf{E}_2.$$

(KF3c) Compute the prior mean and variance matrix of $(\mathbf{X}_i | \mathbf{y}_{i-1})$

$$\begin{aligned} \boldsymbol{\mu}_i &= \varphi_i + \mathbf{C}(s_{i-1}, s_i) \mathbf{m}_{i-1}^*, \quad \varphi_i = \varphi(s_i), \quad s_i = s_{i-1} + \Delta t_i, \quad \Delta t_i = t_i - t_{i-1} \\ \Sigma_i &= \mathbf{C}(s_{i-1}, s_i) \mathbf{S}_{i-1}^* \mathbf{C}(s_{i-1}, s_i)^T + \mathbf{V}(s_{i-1}, s_i) \end{aligned}$$

(KF3d) Compute $\boldsymbol{\mu}_i^Y = \mathbf{B} \boldsymbol{\mu}_i$, $\Sigma_i^Y = \Sigma_i + \Sigma_e$. **Output:** $P(\mathbf{y}_i | \mathbf{y}_{i-1}; \boldsymbol{\theta}) = P_N(\mathbf{y}_i | \boldsymbol{\mu}_i^Y, \Sigma_i^Y)$.

As we illustrate in Figure 2, in steps (KF2) and (KF3d) we used the observation equation to derive the likelihood terms. In step (KF3a), we used Bayes rule to derive the posterior distribution, and in steps (KF3c) the transition equations. In step (KF3b), the phase correction in (3.8) is performed using the Euclidean distance, which implies that the transversal sections are orthogonal to the tangent vectors $\mathbf{F}(\varphi)$ in (3.2). A Newton-Raphson algorithm is used to find the point $\varphi(s_{i-1})$ as in (3.8). The posterior distributions $(\boldsymbol{\kappa}_{i-1} | \mathbf{y}_{i-1})$ are then projections (on the orthogonal transversal section) of the conditional distribution of the noise $(\boldsymbol{\xi}_{i-1} | \mathbf{y}_{i-1})$, with $\boldsymbol{\xi}_{i-1}$ as in (3.14).

Multiple time-series

Typically data consist of multiple independent time-series of observations, possibly with observations taken at different time-points. In this case, the joint likelihood of the multiple time-series is simply the product of the likelihood of each time-series that can be computed based on the above Kalman Filter. If the same initial condition is used for all time-series, then the LNA system in eqs. (3.2), (3.5) and (3.6) needs to be solved only once for all time-series. This assumption might be suitable when the experimental design implies that the oscillating system is initialised in the same experimental conditions. For instance, for the NF- κ B system that we consider, each time-series correspond to different cells. These cells at the initial time-point are left at resting state for an appropriate time

interval before applying an activating signal. The noise around the initial condition is incorporated into the model by the distribution of ξ_0 . Therefore, the use of the same initial conditions is not only appropriate but also preferable because it allows us to draw inference for them from the data. Alternatively, the initial conditions might differ only by their phase in the oscillating cycle. Again the LNA system can be solved once and the phase of the system at the initial time-point can be identified by phase correction.

Finally, if the initial conditions differ vastly one might wish to use a different initial condition for each time-series with additional computational cost.

3.2 Markov chain Monte Carlo algorithms

We implement a Bayesian analysis to conduct inference on the selected parameters within the model systems. Previous analyses of smaller systems (e.g. [Girolami and Calderhead, 2011](#); [Burton et al., 2021](#)) have shown that the choice of inference algorithm can severely impact the efficiency of the parameter estimation for even relatively small dynamical systems. The likelihood of time-series observations is derived through the Kalman Filter and has the form of a product of conditional Gaussian densities as explained above. It's not possible to derive the full conditional distributions for the parameters due to the complex dependence of the likelihood to the parameters and therefore we cannot utilise Gibbs samplers to conduct inference.

Due to the nature of the dynamics of the systems, previous studies have found significant problems of poor mixing in chains when conducting analyses on small stochastic systems (e.g. [Fearnhead et al., 2014](#)).

To overcome these challenges, we implement three different Monte Carlo algorithms, namely a parallel-tempered Random Walk algorithm ([Gupta et al., 2018](#)) and a simplified manifold Metropolis adjusted Langevin algorithm ([Girolami and Calderhead, 2011](#)), with a random walk Metropolis algorithm used as a baseline comparison.

Random Walk Metropolis algorithm

The first baseline approach used a random walk Metropolis algorithm, with proposal distribution $q(\cdot)$ set as a multivariate Gaussian distribution centered on the current parameter vector θ^t and with diagonal covariance matrix $\Sigma = \sigma^2 \mathbf{I}$. The proposal variances were specified on the same order of magnitude as the simulated parameter value. Multivariate new parameter values θ^{t+1} are subsequently drawn from the proposal distribution, and are accepted jointly with probability $\alpha(\theta^t, \theta^{t+1})$.

Due to the general properties of MH algorithms to get stuck in local modes, especially in high-dimensional problems or multimodal densities, alternative algorithms were also tested.

Simplified Manifold MALA

[Girolami and Calderhead \(2011\)](#) propose geometric MCMC algorithms, that use a met-

ric tensor $\mathbf{G}(\theta)$ specified on the target posterior distribution to move efficiently around parameter space. Using the local geometric structure of the target around the current parameter value, proposed moves are made along a manifold in the multivariate space to move more swiftly towards regions of high posterior probability. Multiple variants of traditional MCMC methods are proposed, however the approach used here is a manifold algorithm using an approximation to the Fisher information matrix as the metric tensor $\mathbf{G}(\theta)$, based on the mean component of the Kalman-Filter likelihood.

The proposal distribution utilised, $q(\theta)$, is then

$$N\left(\theta + \frac{\epsilon^2}{2}\mathbf{G}^{-1}(\theta)\nabla_{\theta}\mathcal{L}\{\theta_t\}, \epsilon^2\mathbf{G}^{-1}(\theta)\right)$$

where ϵ is tuned to provide reasonable acceptance rates.

Taking account of the higher order geometric structure of the posterior within the proposal has shown considerable improvements in effective sdosele size, albeit at a significant computational cost of calculating the system derivatives ([Girolami and Calderhead, 2011](#)). We test the simplified manifold MALA as a trade-off between computational efficiency and speed as it only requires the first-order partial derivatives of the likelihoods to be calculated.

Parallel tempering

A feasible solution to attempt to circumvent the problem of local modes is trying to run a population of Markov chains in parallel, each with possibly different, but related stationary distributions. Information exchange between distinct chains enables the target chains to learn from past sdoseles, improving the convergence to the target chain ([Gupta et al., 2018](#)).

Parallel tempering (PT) is an algorithm that attempts periodic swaps between multiple Markov chains running in parallel at different temperatures, where sdoseles with shallower energy landscape can traverse between multiple modes more efficiently. Each chain is equipped with an invariant distribution connected to an auxiliary variable, the temperature β , which scales the shallowness of the energy landscape, and hence defines the probability of accepting an unsuitable move ([Gupta et al., 2018](#); [Hansmann, 1997](#)). An increase in the temperature eases the traversal of the sdosele space. High temperature chains accept unfavourable moves with higher probability. As a result, higher temperature chains allow circumvention of local minima, improving both convergence and sdosele efficiency ([Chib and Greenberg, 1995](#)).

Defining the energy $E[\theta^*]$ as the negative log-posterior evaluated at that parameter value, the Parallel Tempering algorithm for a parameter vector θ can be illustrated as follows.

- For $s = 1, \dots, S$ swap attempts
 1. For $j = 1, \dots, J$ chains

- I. For $t = 1, \dots, N_{iter}$ iterations
 - i Propose a new parameter vector θ^* from a symmetric distribution $q(\theta^*|\theta)$
 - ii Calculate the energy $E[\theta^*]$
 - iii Set $\theta_{t+1} = \theta^*$ with probability $\min(1, e^{-\beta_j \Delta E_j})$, where $\Delta E_j = E_j[\theta^*] - E_j[\theta_{t-1}]$. Otherwise, set $\theta_{t+1} = \theta_t$.
 - II. Record the value of the parameters and the energy on the final iteration
2. For each consecutive pair of chains (in decreasing order of temperature)
 - I. Accept swaps with probability $\min(1, e^{-\Delta\beta \Delta E})$, where $\Delta E = E_j - E_{j-1}$ and $\Delta\beta = \beta_j - \beta_{j-1}$.

If $\beta_c = 1$, then the exact posterior distribution of interest is being sampled, hence, samples of the chain where $\beta_c = 1$ are retained and summary statistics calculated, with other chains used for improving convergence and subsequently discarded.

4 Simulation studies

4.1 System analysis and identifiability

System sensitivity analyses were performed for the two exemplar models using Fisher Information around the values of parameters reported in the literature as broadly representing the system dynamics. The analyses, which are shown in Figure 3, examine both the absolute and relative sensitivity of the model through the eigenvalues of the FIM, but also the model sensitivity to changes in the values of each parameter.

The singular values of the FIM of the NF- κ B system with parameter changes in the log-scale are substantially larger than all other systems indicating a generally higher sensitivity in this model (see Figure 3a). However, the relative sensitivity of the same system is worse than any other considered system as the first two singular values dominate the magnitude of the FIM (see Figure 3b). The circadian clock model for both values of Ω exhibits a slow decrease in the first ten singular values of the system, which is translated as relatively small differences in the sensitivity of the model in a much larger number of directions of the parameter space, compared to the NF- κ B system. This suggests that the circadian clock will provide better mixing of the MCMC chains since the changes in the likelihood over the parameter space are more smooth compared to the NF- κ B system. In contrast, the sharp decrease of the singular values of the NF- κ B system indicate that the likelihood is much more sensitive to changes in a small number of directions of the parameter space (one for the log-scale and two for the raw scale) compared to any other direction.

From the sensitivity analysis, it is apparent that the two parameters associated with the two largest singular values of the NF- κ B system in the raw scale were those corresponding to the mRNA synthesis rates for the variables $I\kappa B\alpha$ and A20, namely $c1$ and $c1a$ respectively (notice the white and black color for those parameters in the heatmap in Figure 3b). Different parameters were highlighted as sensitive on the log-scale, with

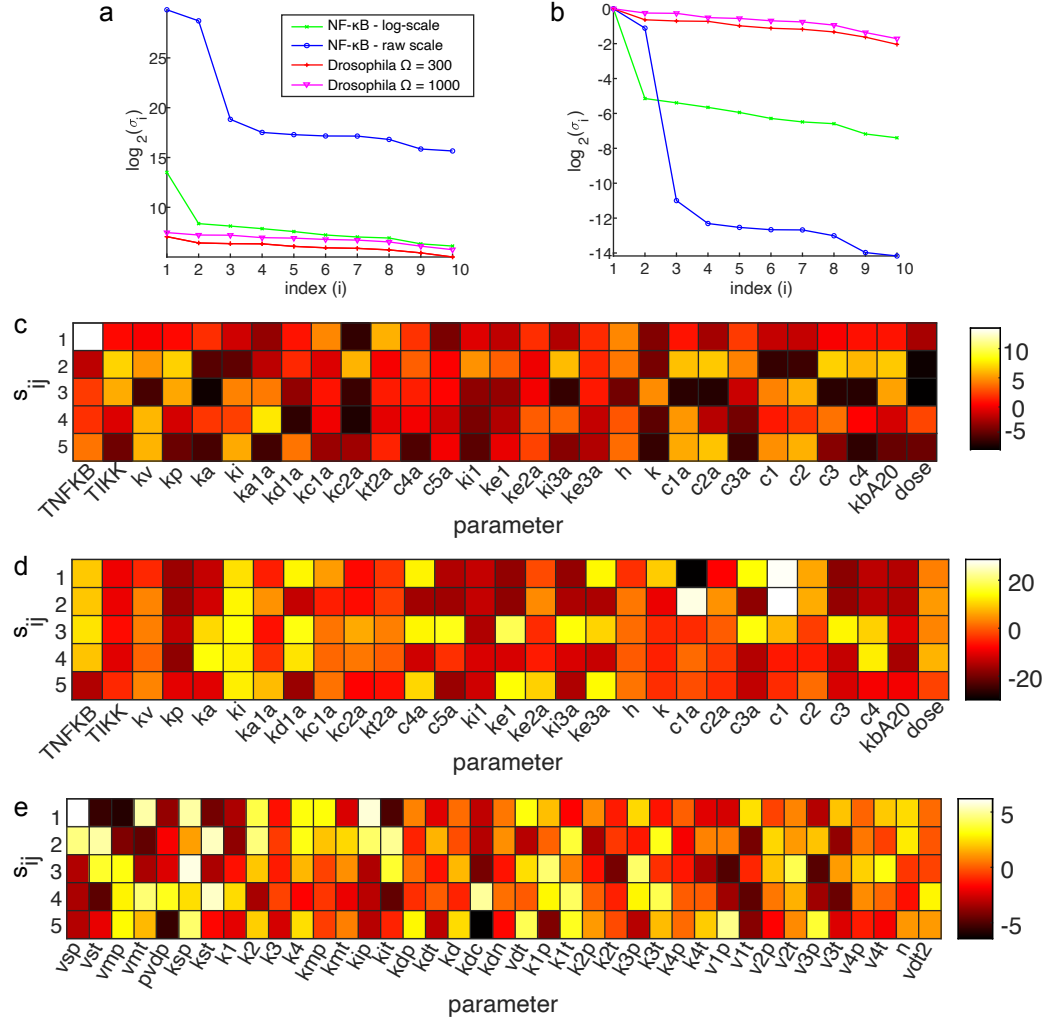


Figure 3: Sensitivity analysis for the pCLNA model of the two exemplar systems. (a-b) The singular values of the FIM of the two exemplar systems. Plot (a) compares the FIM of NF- κ B system in the log-scale and the raw scale of parameters with the FIM of the Drosophila circadian clock model for two values of the system size Ω . Plot (b) Compares the normalised (divided by the largest singular value of the same FIM for the same models). The NF- κ B system overall has larger sensitivities, but the FIM is dominated by few eigen-directions, while the clock model is more balanced in parameter sensitivities. Plots (c-e) are heatmaps of the sensitivity coefficients (in log case, base 2), s_{ij} , as in (2.3) for (c) the parameters of the NF- κ B system in log-scale, (d) the parameters of the NF- κ B system in raw scale (e) the parameters of the Drosophila circadian clock system ($\Omega = 300$). Fewer parameters stand out as having substantially higher or substantially lower sensitivity coefficients than the rest of the parameters in the NF- κ B system compared to the circadian clock.

higher sensitivity coefficients primarily for total NF- κ B concentration (TNFKB), and secondly for (TNF α) *dose* and few others.

The slow decay in singular values of the *Drosophila* circadian clock suggests that a larger number parameters could be estimable than those in the NF- κ B model. In particular, the sensitivities coefficients suggest that parameters *vsp*, *vst*, *vmp*, *vmt*, *pdpv*, *ksp*, *kst*, *kip* and *kit* could be estimable.

We used these sensitivity analyses to guide the initial choice of parameters to estimate within the Bayesian inferential framework. Other parameters not included in the inference are fixed at the respective values from the literature, both due to the fact that the model is relatively insensitive to these parameters and therefore less affected by incorrect choices of these parameters and that the data are unlikely to be able to constrain these parameters.

4.2 Parameter estimates and identifiability

For each of the different settings, ten independent stochastic trajectories were generated using either the pcLNA simulation algorithm (Minas and Rand, 2017) or the full SSA, with parameters fixed at those from available literature (Ashall et al., 2009; Gonze et al., 2003). This is a modest sdosele size for typical experiments of those systems.

Each of the three Markov chain Monte Carlo algorithms were run with 20000 iterations, the first 10000 being discarded as burn-in. For the parallel tempering algorithm, $k = 4$ parallel chains were run with $\beta_k \in \{1, 0.75, 0.5, 0.25\}$. Prior distributions were specified on each of the rate parameters on the raw scale, whilst inference was conducted both on the raw scale and on the log scale with appropriate Jacobian term applied to the acceptance probabilities in the case of the latter. Relatively vague Gamma(1,10) priors were specified on rate parameters and inverse Gamma IG(0.001,0.001) for the error variance.

NF- κ B system

Each of the three Markov chain Monte Carlo algorithms were initially run for the NF- κ B system with two unknown parameters (*c1a* and *c1*) identified from the sensitivity analysis, with other parameters fixed at values from the literature. Posterior summary plots for the three algorithms are shown in 4. All three of these algorithms appeared to converge relatively quickly, and were centered on the true parameter values. Effective sample sizes were calculated for each of the three methods, with the geometric algorithm unsurprisingly showing on average a 35% improvement relative to the random walk Metropolis algorithm. The parallel tempering algorithm on average had a 52% reduction in ESS relative to the random walk algorithm. The main difference in posteriors between the three algorithms were observed in the parallel tempering algorithm, where a second mode close to zero was also occasionally visited by the the main chain. Although the initial chains look like they converged, clearly the smaller mode of the posterior was not visited by either of the two algorithms, hindered by the low-probability region between the two modes.

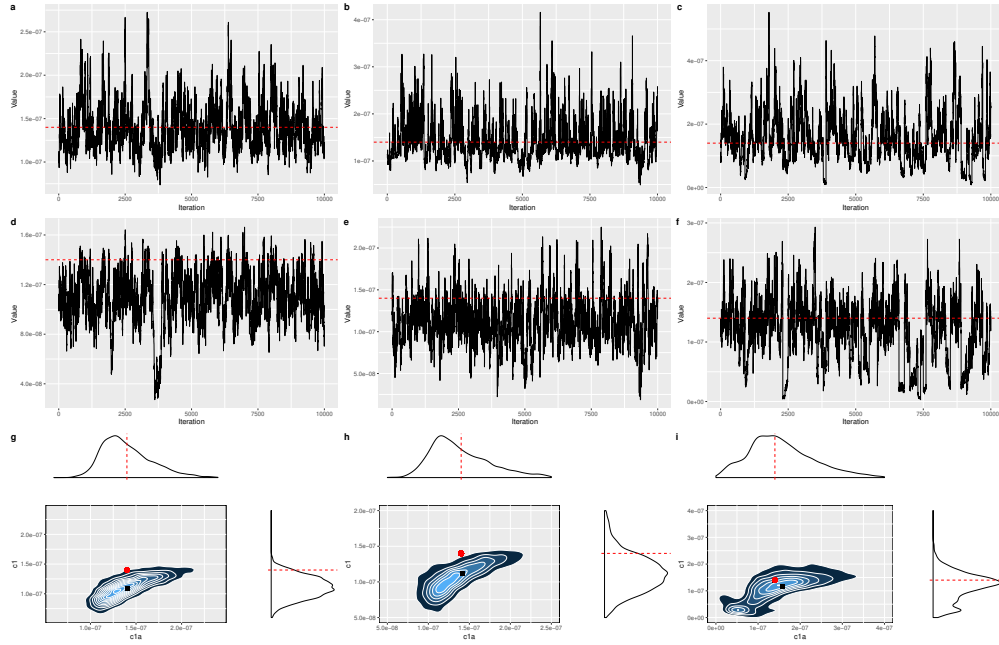


Figure 4: Posterior inference post-burn-in for parameters $c1a$ and $c1$ in the NF- κ B system, conducted on the original parameter scale. Top two rows show traceplots for parameter $c1a$ and $c1$ respectively with the bottom row showing bivariate marginal distributions. Each column relates to a single algorithm type (random walk Metropolis, SMMALA and parallel tempered random walk). Red dashed lines/circles correspond to the true parameter values and yellow circles the posterior mean.

Parameter	Algorithm	Truth	Post. mean	95% HPDI	
$c1a$	RWM		$1.41e^{-7}$	$9.28e^{-8}$	$1.98e^{-7}$
	SMMALA	$1.4e^{-7}$	$1.42e^{-7}$	$7.45e^{-8}$	$2.26e^{-7}$
	PT		$1.57e^{-7}$	$1.08e^{-8}$	$3.08e^{-7}$
$c1$	RWM		$1.09e^{-7}$	$7.15e^{-8}$	$1.50e^{-7}$
	SMMALA	$1.4e^{-7}$	$1.12e^{-7}$	$5.76e^{-8}$	$1.76e^{-7}$
	PT		$1.16e^{-7}$	$1.50e^{-8}$	$2.05e^{-7}$

Table 1: Posterior summary statistics for the Drosophila clock with $\Omega = 300$

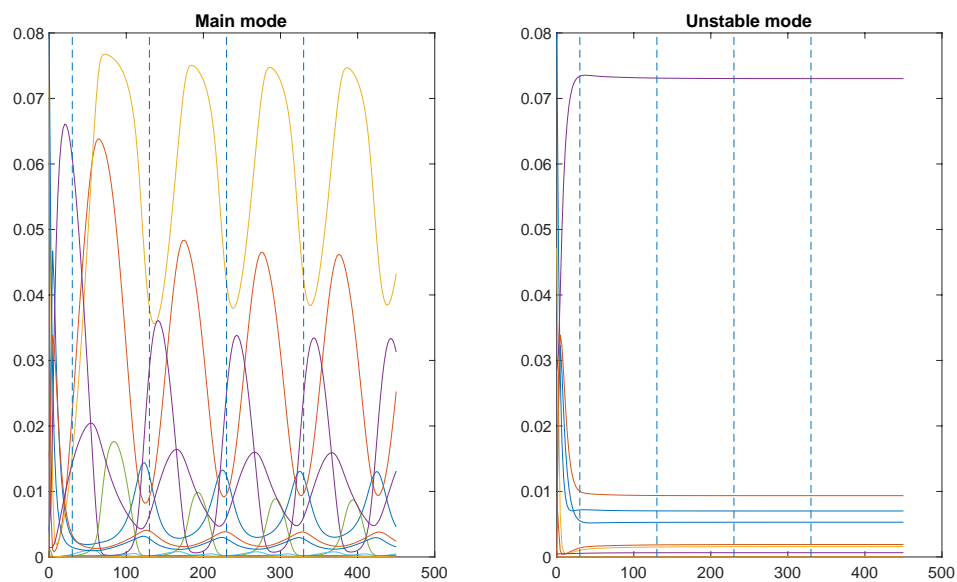


Figure 5: Deterministic solutions of the NF- κ B ODE system evaluated at the two posterior modes highlighted by the parallel tempering algorithm. The left plot corresponds to a value close to the correct values, whilst the right plot corresponds to values close to zero giving no oscillations beyond the first peak. The vertical dashed lines correspond to the observation times.

This second mode observed in the parallel tempering analysis was studied further to determine possible reasons that the tempered algorithm visited this mode and the biological implications of this. Figure 5 shows the deterministic solution to the system with parameters $c1a$ and $c1$ at the values from the literature and also again when replaced with the mean of this lower mode. This shows a clear problem with the discrete timepoints used for inference, as the observation times traditionally measured correspond only to the peaks of the nuclear NF- κ B. In this case, the algorithm correctly fails to reject parameters that give deterministic model solutions without oscillations as the level of nuclear NF- κ B remains constant at a similar level to the peak height in the oscillatory system. Biologically, this corresponds to a system with zero feedback between the corresponding variables.

As the parallel tempered algorithm was the only algorithm to effectively explore the multimodal parameter space, all further analyses were conducted using this algorithm. We further varied the parameter settings in the following ways.

Log-scale inference

The sensitivity analysis also showed variability depending on whether the parameters were transformed or not prior to conducting analysis. Whilst parameters $c1a$ and $c1$ were the most sensitive on the raw scale, when transforming parameters to a log scale, alternative parameters had higher sensitivity loadings. We therefore also conducted inference on the log parameter scale using these parameters as the basis for inference. Despite this, there is one dominant singular value in the system so it was again expected this would correspond to the number of estimable parameter directions. Specifically, the total concentration of NF- κ B was the dominant parameter, with additional lower sensitivities to parameters (TNF α) dose and $kbA20$. Additional parameters with much lower sensitivities, namely $kc1a$ and $c5a$, were included to test how these would behave in the inference. The total NF- κ B parameter determines the overall levels of all variables in the system. Prior distributions were kept similar to those in the previous analysis, specified on the un-transformed scale, but an appropriate Jacobian term was introduced into the Metropolis acceptance step to ensure the correct invariant distribution was reached. In the case of the log transform with prior specified on the raw scale, the log posterior is $\log(\pi(\theta|y)) \propto \log(f(y|\theta)) + \log(p(\log(\theta))) - \log(\theta)$, where the final term is the Jacobian of the log transformation.

In each case, four chains were again run in parallel, with 20000 iterations consisting of 200 swaps in total, with swaps proposed every 100 iterations. The β parameters across four chains were set at $\beta \in [1, 0.5, 0.2, 0.1]$. Table 2 presents posterior summaries of the results, in which the parameters can be reliably estimated. Posterior means were very close to the true parameter values, with all 95% HPDIs containing the true value for all parameters.

Unobserved variables

Further analyses were run under the setting that measurements of some of the biological species are not easily obtained experimentally. In this case, the matrix \mathbf{B} in the Kalman

Parameter	Truth	Post. mean	95% HPDI	
TNFKB	0.080	0.080	0.079	0.081
<i>kc1a</i>	0.074	0.115	0.072	0.186
<i>c5a</i>	$2.2e^{-5}$	$1.50e^{-4}$	$1.77e^{-5}$	$3.05e^{-4}$
<i>kbA20</i>	0.002	0.002	0.001	0.002
<i>dose</i>	1.000	1.026	0.890	1.240
σ	0.000	0.000	0.000	0.000

Table 2: Posterior estimates to 3d.p. for the NF κ B system with parameter inference conducted on the log-scale and all 11 variables measured.

Parameter	Truth	Post. mean	95% HPDI	
<i>TNFKB</i>	0.080	0.079	0.066	0.092
<i>kc1a</i>	0.074	1.191	0.006	2.218
<i>c5a</i>	$2.2e^{-5}$	$3.69e^{-4}$	$9.88e^{-5}$	$6.79e^{-4}$
<i>kbA20</i>	0.002	0.007	0.001	0.016
<i>dose</i>	1.000	10.623	2.845	19.595
σ	0.000	0.000	0.000	0.000

Table 3: Posterior estimates for the NF κ B system with parameter inference conducted on the log-scale and only four variables measured.

filter is no longer an identity matrix, but contains some zero elements along the diagonal also. Table 3 shows the results for the same set-up as Table 2 but assuming only nuclear and cytoplasmic NF- κ B, cytoplasmic I κ B α and A20 are measurable.

The parallel tempered algorithm converged similarly in this case, but the ability to estimate some of the parameters deteriorated. Specifically, the dose parameter reverted to the prior mean of approximately 10 and the estimate of parameter *kc1a* was positively biased towards the prior mean. The other parameters did not appear to be greatly impacted by the reduced measurement matrix.

Drosophila clock

Analyses were also conducted using the Drosophila circadian clock system with similar settings to those in the NF- κ B system. Parameters selected for inference corresponded to those with highest sensitivity loadings. As noted previously, the clock system has higher sensitivities to a larger number of parameters and hence here nine parameters were estimated. For the Drosophila clock, data were simulated directly from the Gillespie algorithm (SSA) to confirm the correct stochastic trajectories can still be obtained when fitting to the exact algorithm. It would be expected that results under this setting could perform worse due to any potential discrepancies between the approximation of the stochastic dynamics using the linear noise approximation and the exact stochastic algorithm. Prior distributions for the rate parameters were set as Gamma(1,10). Trace plots are shown in Figure 6 for the nine parameters in addition to the error standard

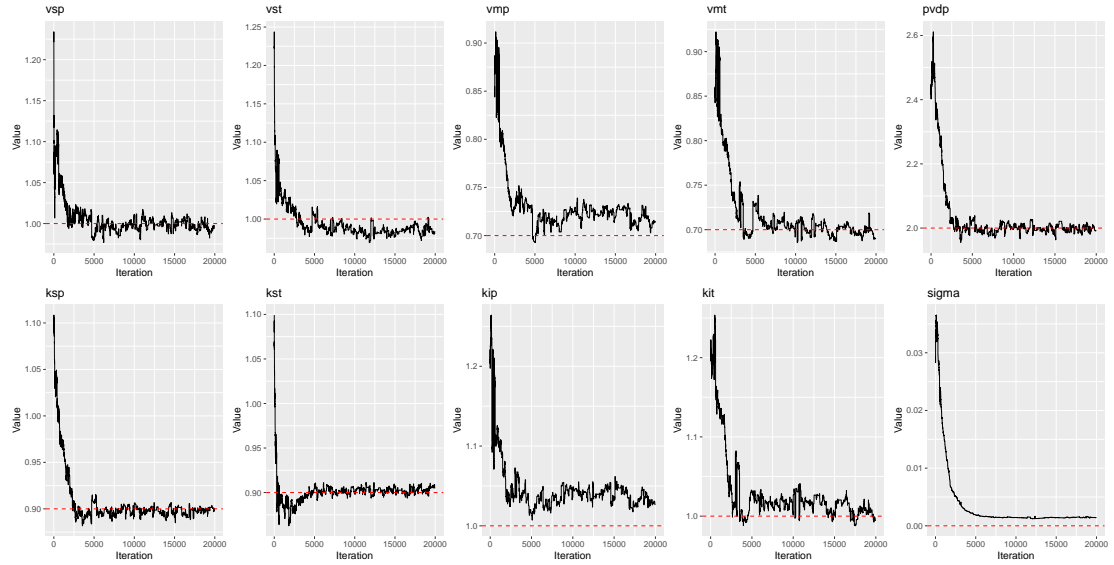


Figure 6: Posterior inference for the *Drosophila* circadian clock system estimating 9 parameters. Dashed horizontal line corresponds to the true parameter value used to simulate the data.

Parameter	Truth	Post. mean	95% HPDI	
<i>vsp</i>	1.000	0.999	0.987	1.009
<i>vst</i>	1.000	0.984	0.975	0.998
<i>vmp</i>	0.700	0.722	0.707	0.732
<i>vmt</i>	0.700	0.700	0.687	0.713
<i>pvdp</i>	2.000	1.999	1.976	2.021
<i>ksp</i>	0.900	0.898	0.890	0.906
<i>kst</i>	0.900	0.903	0.896	0.909
<i>kip</i>	1.000	1.038	1.023	1.052
<i>kit</i>	1.000	1.013	0.994	1.035
σ	0.000	0.001	0.001	0.002

Table 4: Posterior summary statistics for the estimated parameters in the *Drosophila* circadian clock with $\Omega = 1000$.

Parameter	Truth	Post. mean	95% HPDI	
vsp	1.000	1.000	0.960	1.028
vst	1.000	1.052	1.035	1.077
vmp	0.700	0.768	0.705	0.794
vmt	0.700	0.851	0.819	0.890
pvdv	2.000	2.041	1.986	2.097
ksp	0.900	0.919	0.896	0.938
kst	0.900	0.912	0.896	0.926
kip	1.000	1.152	1.097	1.176
kit	1.000	1.181	1.142	1.231
sigma	0.000	0.013	0.011	0.014

Table 5: Posterior summary statistics for the estimated parameters in the *Drosophila* circadian clock with $\Omega = 300$.

deviation and Table 4 shows posterior summary statistics. All estimates were very close to the true values, with credible interval coverage being high. The estimation of an additional observational error may explain some of the small discrepancies in parameter estimates, although the magnitude is negligible.

Varying stochasticity

In the case of a higher value of the system size, $\Omega = 1000$, which leads to a system with lower stochasticity, we were able to correctly estimate the nine simulated parameters with high precision. When stochasticity was higher, namely $\Omega = 300$, reasonable estimates of the parameters were still obtained (Table 5) but slightly higher bias in the posterior estimates and credible intervals were observed. The observation error variance was also inflated in this case.

5 Discussion

The proposed approach was highly successful in retrieving accurate estimates of simulated parameters from data in large stochastic non-linear dynamical systems with oscillations, conditional on the level of sensitivity of the model output to those parameters being sufficiently high. The sensitivity analysis was able to predict which parameters were estimable from observed data, across the tested simulation settings (different variables, varying Omega and Gillespie and pcLNA simulated data). These highly-parameterised systems have not previously been estimable due to the computational demand of calculating the conditional distributions of the state process at the desired timepoints. Our simulations have highlighted a variety of challenges of the systems, including (non-)identifiability, data resolution and multimodal distributions common to these types of systems.

We emphasise the importance of conducting sensitivity analysis on non-linear dynamical systems prior to conducting inference. Attempting to conduct inference in partially- or non-identifiable systems risks erroneous results, even for parameters that

should be identifiable. In the case of the parallel tempering algorithm, posteriors marginals were similar to the priors specified on them but with too many non-identifiable parameters this may not remain the case. Our results also show the importance of considering the discrete time points that are used to conduct inference. In some instances these may be determined by the experimental set-up, but as modern sequencing technologies continue to advance, the choice of resolution and interrogation of the underlying continuous process will be increasingly important. Sensitivity analyses or inference should also allow for varying temporal resolutions in the data ([Baggenstoss, 2018](#), e.g.), particularly in the presence of observation errors.

We compared several MCMC algorithms for conducting inference and found that despite improvements in effective sample sizes, the random walk Metropolis and geometric algorithms struggled to bypass bifurcations in parameter space and hence underestimate posterior uncertainty in marginal distributions. Our approach using the tempered algorithm was able to account for bifurcations in parameter space and also highlight alternative parameter combinations consistent with the data that warranted further study. [Girolami and Calderhead \(2011\)](#) highlight that extending the manifold MALA algorithm to a manifold Hamiltonian Monte Carlo (HMC) algorithm facilitates implementation within a parallel tempered algorithm and this may further improve the results found here. In particular, the improved convergence rate of parallel tempering combined with the improved local mixing of the geometric algorithms. It should be noted, however, that this does require significant increased computational power in the calculation of the derivatives of the metric tensor (i.e. FIM) and improvements in efficiency could be hindered by this.

We have shown that the ability to estimate parameters accurately and precisely varies along a variety of axes within these stochastic models. Increasing number of large eigenvalues of the mechanistic model is shown empirically to be proportional to the number of estimable parameters in the model and the loadings of the principal eigenvalues are highly indicative of which parameters are estimable. Similarly, increasing stochasticity unsurprisingly hindered the ability to obtain more precise parameter estimates via uncertainty in the corresponding posterior marginals. In many experimental designs, it may not be feasible to measure all of the biological species and our results show this can hinder the estimation of some parameters, but others are still estimable if the sensitive outputs are still measured.

Our approach has made significant advances in the ability to conduct exact and fast Bayesian inference in high-dimensional stochastic systems of reaction networks, whilst being similarly applicable to other stochastic models based on stochastic differential equations, such as those found in epidemiology and population dynamics. Remaining challenges exist in improving optimal experimental design, as well as developing optimum block updating strategies for the parameters when single parameters may dominate.

Acknowledgement

BS acknowledges funding from BBSRC grant BB/K003097/1 and the Edinburgh Mathematical Society

References

- Allen, L. J. S. (2017). “A primer on stochastic epidemic models: Formulation, numerical simulation, and analysis.” *Infectious Disease Modelling*, 2: 128–142.
 URL <http://www.ncbi.nlm.nih.gov/pubmed/29928733><http://www.pubmedcentral.nih.gov/articlerender.fcgi?artid=PMC6002090> 2
- Ashall, L., Horton, C. A., Nelson, D. E., Paszek, P., Harper, C. V., Sillitoe, K., Ryan, S., Spiller, D. G., Unitt, J. F., Broomhead, D. S., Kell, D. B., Rand, D. A., Sée, V., and White, M. R. H. (2009). “Pulsatile Stimulation Determines Timing and Specificity of NF- κ B-Dependent Transcription.” *Science*, 324(5924): 242–246. 1, 2, 4, 15
- Baggenstoss, P. M. (2018). “Acoustic Event Classification Using Multi-Resolution HMM.” In *2018 26th European Signal Processing Conference (EUSIPCO)*, 972–976. 22
- Beaumont, M. A. (2003). “Estimation of Population Growth or Decline in Genetically Monitored Populations.” *Genetics*, 164(3): 1139–1160. 2
- Boettiger, C. (2018). “From noise to knowledge: how randomness generates novel phenomena and reveals information.” *Ecology Letters*, 21: 1255–1267.
 URL <http://doi.wiley.com/10.1111/ele.13085> 2
- Browning, A. P., Warne, D. J., Burrage, K., Baker, R. E., and Simpson, M. J. (2020). “Identifiability analysis for stochastic differential equation models in systems biology.” *Journal of The Royal Society Interface*, 17(173): 20200652.
 URL <https://royalsocietypublishing.org/doi/abs/10.1098/rsif.2020.0652> 3
- Burton, J., Manning, C. S., Rattray, M., Papalopulu, N., and Kursawe, J. (2021). “Inferring kinetic parameters of oscillatory gene regulation from single cell time-series data.” *Journal of The Royal Society Interface*, 18(182): 20210393. 11
- Chib, S. and Greenberg, E. (1995). “Understanding the Metropolis-Hastings Algorithm.” *American Statistician*, 49: 327–335. 12
- DeFelice, M. M., Clark, H. R., Hughey, J. J., Maayan, I., Kudo, T., Gutschow, M. V., Covert, M. W., and Regot, S. (2019). “NF- κ B signaling dynamics is controlled by a dose-sensing autoregulatory loop.” *Science Signaling*, 12. 2
- Fearnhead, P., Giagos, V., and Sherlock, C. (2014). “Inference for reaction networks using the linear noise approximation.” *Biometrics*, 70(2): 457–466. 2, 4, 11
- Finkenstädt, B., Woodcock, D. J., Komorowski, M., Harper, C. V., Davis, J. R. E., White, M. R. H., and Rand, D. A. (2013). “Quantifying intrinsic and extrinsic noise

- in gene transcription using the linear noise approximation: an application to single cell data.” *The Annals of Applied Statistics*, 7(4): 1960–1982. 2, 3
- Forger, D. B. (2017). *Biological clocks, rhythms, and oscillations: The theory of biological timekeeping*. Cambridge (MA): MIT Press. MIT Press, Cambridge (MA). 1
- Froda, S. and Nkurunziza, S. (2007). “Prediction of predator–prey populations modelled by perturbed ODEs.” *Journal of Mathematical Biology*, 54(3): 407–451.
URL <https://doi.org/10.1007/s00285-006-0051-9> 1
- Gabriel, C. H., del Olmo, M., Zehtabian, A., Jäger, M., Reischl, S., van Dijk, H., Ulbricht, C., Rakhymzhan, A., Korte, T., Koller, B., Grudziecki, A., Maier, B., Herrmann, A., Niesner, R., Zemojtel, T., Ewers, H., Granada, A. E., Herzog, H., and Kramer, A. (2021). “Live-cell imaging of circadian clock protein dynamics in CRISPR-generated knock-in cells.” *Nature Communications*, 12: 3796. 2
- Gard, T. C. and Kannan, D. (1976). “On a stochastic differential equation modeling of prey-predator evolution.” *Journal of Applied Probability*, 13(3): 429–443. 1
- Gillespie, D. T. (1977). “Exact stochastic simulation of coupled chemical reactions.” *The Journal of Physical Chemistry*, 81(25): 2340–2361. 2
- (1992). “A rigorous derivation of the chemical master equation.” *Physica A: Statistical Mechanics and its Applications*, 188: 404–425.
URL <http://www.sciencedirect.com/science/article/pii/037843719290283V>
<https://www.sciencedirect.com/science/article/pii/037843719290283V> 2
- (2000). “The chemical Langevin equation.” *The Journal of Chemical Physics*, 113: 297–306.
URL <http://scitation.aip.org/content/aip/journal/jcp/113/1/10.1063/1.481811> 2
- Gillespie, D. T. and Petzold, L. R. (2003). “Improved leap-size selection for accelerated stochastic simulation.” *The Journal of Chemical Physics*, 119. 2
- Girolami, M. and Calderhead, B. (2011). “Riemann manifold Langevin and Hamiltonian Monte Carlo methods.” *Journal of the Royal Statistical Society: Series B (Statistical Methodology)*, 73(2): 123–214. 2, 3, 11, 12, 22
- Goldental, A., Uzan, H., Sardi, S., and Kanter, I. (2017). “Oscillations in networks of networks stem from adaptive nodes with memory.” *Scientific Reports*, 7: 2700. 1
- Gonze, D., Halloy, J., Leloup, J.-C., and Goldbeter, A. (2003). “Stochastic models for circadian rhythms: effect of molecular noise on periodic and chaotic behaviour.” *Comptes Rendus Biologies*, 326(2): 189 – 203. 1, 2, 4, 15
- Gonze, D. and Ruoff, P. (2021). “The Goodwin Oscillator and its Legacy.” *Acta Biotheoretica*, 69: 857–874.
URL <http://link.springer.com/10.1007/s10441-020-09379-8> 1
- Greer, M., Saha, R., Gogliettino, A., Yu, C., and Zollo-Venecek, K. (2020). “Emergence

- of oscillations in a simple epidemic model with demographic data.” *Royal Society Open Science*, 7: 191187. [1](#)
- Grima, R., Thomas, P., and Straube, A. V. (2011). “How accurate are the nonlinear chemical Fokker-Planck and chemical Langevin equations?” *The Journal of Chemical Physics*, 135: 084103. [7](#)
- Gupta, S., Hainsworth, L., Hogg, J., Lee, R., and Faeder, J. (2018). “Evaluation of Parallel Tempering to Accelerate Bayesian Parameter Estimation in Systems Biology.” In *2018 26th Euromicro International Conference on Parallel, Distributed and Network-based Processing (PDP)*, 690–697. [11](#), [12](#)
- Gutenkunst, R. N., Waterfall, J. J., Casey, F. P., Brown, K. S., Myers, C. R., and Sethna, J. P. (2007). “Universally Sloppy Parameter Sensitivities in Systems Biology Models.” *PLoS Comput Biol*, 3: e189.
URL <https://dx.plos.org/10.1371/journal.pcbi.0030189> [3](#)
- Hansmann, U. H. (1997). “Parallel tempering algorithm for conformational studies of biological molecules.” *Chemical Physics Letters*, 281(1): 140 – 150.
URL <http://www.sciencedirect.com/science/article/pii/S0009261497011986> [12](#)
- Harper, C. V., Woodcock, D. J., Lam, C., Garcia-Albornoz, M., Adamson, A., Ashall, L., Rowe, W., Downton, P., Schmidt, L., West, S., Spiller, D. G., Rand, D. A., and White, M. R. H. (2018). “Temperature regulates NF- κ B dynamics and function through timing of A20 transcription.” *Proceedings of the National Academy of Sciences*.
URL <https://www.pnas.org/content/pnas/115/22/E5243.full.pdf> [2](#)
- Ito, Y. and Uchida, K. (2010). “Formulas for intrinsic noise evaluation in oscillatory genetic networks.” *Journal of Theoretical Biology*, 267: 223–234.
URL <http://www.sciencedirect.com/science/article/pii/S0022519310004480> [2](#)
- Komorowski, M., Finkenstädt, B., Harper, C. V., and Rand, D. A. (2009). “Bayesian inference of biochemical kinetic parameters using the linear noise approximation.” *BMC Bioinformatics*, 10(1): 343. [2](#), [3](#)
- Kurtz, T. G. (1970). “Solutions of ordinary differential equations as limits of pure jump markov processes.” *Journal of Applied Probability*, 7(1): 49–58. [2](#)
- Lane, K., Valen, D. V., DeFelice, M. M., Macklin, D. N., Kudo, T., Jaimovich, A., Carr, A., Meyer, T., Pe’er, D., Boutet, S. C., and Covert, M. W. (2017). “Measuring Signaling and RNA-Seq in the Same Cell Links Gene Expression to Dynamic Patterns of NF- κ B Activation.” *Cell Systems*, 4: 458–469.e5. [2](#)
- Lei, J. (2021). *Systems biology : modeling, analysis, and simulation*. Lecture notes on mathematical modelling in the life sciences. Springer Cham. [2](#)
- Marinopoulou, E., Biga, V., Sabherwal, N., Miller, A., Desai, J., Adamson, A. D., and Papalopulu, N. (2021). “HES1 protein oscillations are necessary for neural stem cells to exit from quiescence.” *iScience*, 24: 103198. [1](#)

- Minas, G. and Rand, D. A. (2017). “Long-time analytic approximation of large stochastic oscillators: Simulation, analysis and inference.” *PLOS Computational Biology*, 13(7): 1–23. [2](#), [4](#), [7](#), [8](#), [15](#)
- (2019a). “Parameter sensitivity analysis for biochemical reaction networks.” *Mathematical Biosciences and Engineering*, 16: 3965–3987.
URL <http://www.aimspress.com/article/10.3934/mbe.2019196> [3](#)
- (2019b). “Parameter sensitivity analysis for biochemical reaction networks.” *Mathematical Biosciences and Engineering*, 16(5): 3965. [4](#)
- Rand, D. A. (2008). “Mapping global sensitivity of cellular network dynamics: sensitivity heat maps and a global summation law.” *Journal of The Royal Society Interface*, 5: S59–S69.
URL http://rsif.royalsocietypublishing.org/content/5/Suppl_1/S59.abstract [3](#)
- Schnoerr, D., Sanguinetti, G., and Grima, R. (2017). “Approximation and inference methods for stochastic biochemical kinetics—a tutorial review.” *Journal of Physics A: Mathematical and Theoretical*, 50(9): 093001. [2](#)
- Sisson, S. A., Fan, Y., and Beaumont, M. A. (eds.) (2018). *Handbook of Approximate Bayesian Computation*. Chapman and Hall/CRC. [2](#)
- Tay, S., Hughey, J. J., Lee, T. K., Lipniacki, T., Quake, S. R., and Covert, M. W. (2010a). “Single-cell NF- κ B dynamics reveal digital activation and analogue information processing.” *Nature*, 466: 267–271. [2](#)
- (2010b). “Single-cell NF- κ B dynamics reveal digital activation and analogue information processing.” *Nature*, 466(7303): 267–271.
URL <https://doi.org/10.1038/nature09145> [4](#)
- VAN KAMPEN, N. (ed.) (2007). *Stochastic Processes in Physics and Chemistry (Third Edition)*. North-Holland Personal Library. Amsterdam: Elsevier, third edition edition. [2](#)
- Wallace, E. W. J., Gillespie, D. T., Sanft, K. R., Petzold, L. R., Gillespie, D. T., and Sanft, K. R. (2012). “Linear noise approximation is valid over limited times for any chemical system that is sufficiently large.” *IET SYSTEMS BIOLOGY*, 6: 102–115.
URL <https://digital-library.theiet.org/content/journals/10.1049/iet-syb.2011.0038> [7](#)
- Weitz, J. S., Park, S. W., Eksin, C., and Dushoff, J. (2020). “Awareness-driven behavior changes can shift the shape of epidemics away from peaks and toward plateaus, shoulders, and oscillations.” *Proceedings of the National Academy of Sciences*, 117: 32764–32771. [1](#)
- Wilkinson, D. (2011). *Stochastic Modelling for Systems Biology, Second Edition*. Chapman & Hall/CRC Mathematical and Computational Biology. Taylor & Francis. [2](#)
- Zhang, Q., Lenardo, M. J., and Baltimore, D. (2017). “30 Years of NF- κ B: A Blossoming of Relevance to Human Pathobiology.” *Cell*, 168: 37–57.

URL <https://www.sciencedirect.com/science/article/pii/S0092867416317263> 4